Environmental Pollution 340 (2024) 122803

Contents lists available at ScienceDirect

Environmental Pollution

journal homepage: www.elsevier.com/locate/envpol

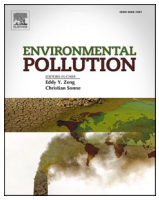

Evaluation of air quality changes in a Chinese megacity over a 15-year period (2006–2021) using $PM_{2.5}$ receptor modelling☆,☆☆

A. Canals-Angerri [a,b,*], W. Lv [c], X. Zhuang [d], Y. Shangguan [d], Y. Wang [e], S. Kong [e], P.K. Hopke [f], F. Amato [a], A. Alastuey [a], B.L. van Drooge [a], X. Querol [a]

[a] Institute of Environmental Assessment and Water Research (IDAEA), CSIC, Barcelona, Spain
[b] Department of Chemical Engineering and Analytical Chemistry, Universitat de Barcelona, Spain
[c] Wuhan Regional Climate Centre, Wuhan, PR China
[d] School of Earth Resources, China University of Geosciences, Wuhan, PR China
[e] School of Environmental Studies, China University of Geosciences, Wuhan, PR China
[f] Department of Public Health Sciences, University of Rochester School of Medicine and Dentistry, Rochester, NY, USA

ARTICLE INFO

Keywords:
Atmospheric particulate matter
Urban background
Wuhan
Geochemistry
Source apportionment
$PM_{2.5}$

ABSTRACT

Air quality impairment has a massive impact on human health, with atmospheric particulate matter (PM) playing a major role. The People's Republic of China experienced a trend of increasing $PM_{2.5}$ concentrations from 2000 to 2013. However, after the application of the Air Pollution Prevention and Control Action Plan and other related control measures, sharp decreases in air pollutant concentrations were particularly evident in the city of Wuhan (central China). This study analysed major changes in $PM_{2.5}$ concentrations, composition and source apportionment (using receptor modelling) based on Wuhan's $PM_{2.5}$ chemical speciation datasets from 2006 to 2007, 2019–2021 and contemporaneous gaseous pollutant values. Average SO_2 concentrations decreased by 88%, from the first to the second period, mostly due to measures that reduced coal combustion. However, NO_2 only declined by 25%, with policy measures likely being undermined by an increased number of vehicles. $PM_{2.5}$ concentrations decreased by 65%, with the PM constituents each being affected differently. Coal combustion-related element concentrations, OC, SO_4^{2-}, NH_4^+, EC, Cl^-, Al, Ca, Cu, Fe, Co and NO_3^- decreased by 22–90%. Secondary inorganic aerosol (SIA) was initially dominated by $(NH_4)_2SO_4$ (73%) in 2006, but later dominated by NH_4NO_3 (52%) in 2021. Receptor modelling identified major sources contributing to $PM_{2.5}$: Mineral, road and desert dust (MRDD), Secondary sulphate (SECS), Secondary nitrate (SECN), Tungsten industry (W), Toxic Elements of Coal (TEC), Iron and Steel (IRONS), Coal Combustion (CC), Residential Heating (RH), Refinery (REF) and Traffic (TRF). In relative proportions, TEC (−83%), SECS (−64%) and SECN (−48%) reduced their contributions to $PM_{2.5}$ whilst MRDD increased (+62.5%). Thus, the results indicate not only a drastic abatement of PM pollution in Wuhan but also a change in the sources of pollution, which requires further actions to reduce $PM_{2.5}$ concentrations to health protective values. Secondary PM and fugitive emissions are key components to abate.

☆ This paper has been recommended for acceptance by Pavlos Kassomenos☆☆ Urban background $PM_{2.5}$ concentrations decreased from 129 μg m^{-3} in 2006–2007 to 52 μg m^{-3} in 2019–2021. Receptor modelling was performed for those two differentiated periods and identified nine and five major sources contributing to $PM_{2.5}$, for 2006–2007 and 2019–2021, respectively. Named Mineral, road and desert dust (MRDD), Secondary sulphate (SECS), Secondary nitrate (SECN), Tungsten industry (W), Toxic Elements of Coal (TEC), Iron and Steel (IRONS), Coal Combustion (CC), Residential Heating (RH), Refinery (REF) and Traffic (TRF). Both periods show four source profiles in common and, in absolute concentrations, contributions were markedly reduced from 2006 to 2021. However, in relative proportions, TEC (−83%), SECS (−64%) and SECN (−48%) reduced their contributions to $PM_{2.5}$ between 2006 and 2021 whilst MRDD increased (+62.5%). The relative contributions of TRF, CC, RH, REF and IRONS where no more identified as major sources in the 2019–2021 PMF analysis. Thus, the relative contributions of nitrate-, traffic-, energy- and industry-related $PM_{2.5}$ decreased their relative contributions while those from construction and MRDD increased.

* Corresponding author. Institute of Environmental Assessment and Water Research (IDAEA), CSIC, Barcelona, Spain.
E-mail address: acageo@cid.csic.es (A. Canals-Angerri).

https://doi.org/10.1016/j.envpol.2023.122803
Received 30 May 2023; Received in revised form 5 October 2023; Accepted 23 October 2023
Available online 25 October 2023

1. Introduction

According to the World Health Organization (WHO, 2021), exposure to air pollution is estimated to cause 7 million premature deaths every year. Among the air pollutants causing this large health impact, fine suspended particulate matter ($PM_{2.5}$, atmospheric particulate matter with an aerodynamic diameter <2.5 μm) is one of the largest contributors (GBD, 2020; WHO, 2013) driving health-related costs, which have reached 4.5% of global GDP (World Bank, 2016a, 2016b).

According to the (WHO, 2022), the average (min-max) $PM_{2.5}$ concentration in urban China was 49 (25–99) μg m^{-3} in 2010, resulting in China having the 22nd highest $PM_{2.5}$ pollution level among 194 countries. According to the same dataset, in 2016, the mean concentration remained 49 (48–53) μg m^{-3}, although the range narrowed. Then, China held the 28th position in the ranking. Thus, $PM_{2.5}$ remained relatively high in urban China, exceeding the levels recorded in most urban environments in Europe and the US by a factor of five.

Geng et al. (2021) found that $PM_{2.5}$ in China increased slightly from 2000 to 2006 due to a weak emissions control policy, while a sharp drop in $PM_{2.5}$ concentrations occurred after 2013 when strict control measures were implemented. A peak in $PM_{2.5}$ concentration occurred in 2006, the first year of the 11th Five-Year Plan (2006–2010). The 2013 decrease was the result of the implementation of the Air Pollution Prevention and Control Action Plan (2013–2017) and the Blue Sky Protection Campaign (2018–2020). (Zhai et al., 2019) reported a general decrease in annual mean $PM_{2.5}$ across China of 30–50% over the 2013–2018 period, with a meteorology-corrected trend of −4.6 μg m^{-3} yr^{-1}.

This downward $PM_{2.5}$ trend was very evident in Wuhan, central China, where, according to Lv (2008), the official average $PM_{2.5}$ concentrations at the three air quality monitoring stations in 2006–2007 were 114–130 μg m^{-3}, while 48 μg m^{-3} was reported for 2016–2018 by Ren et al. (2021) for the 20 air quality monitoring stations of the 13 districts of the city. This accounts for a $PM_{2.5}$ decrease of 60% over the 2007–2017 period, with a rate (without meteorological correction) of −3.6 μg m^{-3} yr^{-1}. Yin et al. (2020) reported $PM_{2.5}$ data from 2012 to 2017 from Wuhan and concluded that maximum $PM_{2.5}$ concentrations were recorded in 2013, with an average annual concentration close to 100 μg m^{-3}. From then, a progressive decrease to 50 μg m^{-3} in 2017 occurred. However, $PM_{2.5}$ data for 2000–2011 were unavailable. In the same study, $PM_{2.5}$ speciation results reported by 10 studies of Wuhan were reviewed. It is worth to highlight that since 2016 the $PM_{2.5}$ Chinese annual standards for cities (Class 2) is fixed at 35 μg m^{-3}, according to GB3095-2012 (MEP, 2012). Before this, only PM_{10} levels were included in the standards.

A previous $PM_{2.5}$ sampling campaign was performed by Lv (2008) from July 2006 to July 2007. Chemical analysis and source apportionment were simultaneously implemented at three sites throughout the city (Changqian industrial, Huaqiao urban background and Gaoxin-industrial/urban).

The present study aimed to analyse major changes in $PM_{2.5}$ concentrations, composition and source apportionment in Wuhan City after the application of the Air Pollution Prevention and Control Action Plan and other related pollution control measures. The comparison will be based on the unpublished 2006–2007 $PM_{2.5}$ speciation data by Lv (2008), the one obtained following the same procedure in 2019–2021, and the datasets of gaseous pollutants measured simultaneously. These long-term $PM_{2.5}$ very complete speciation data was very scarce in 2006–2007 in China, but especially in Wuhan. Thus, this work is based on the comparison of these periods using experimental data.

2. Study area

Wuhan (29°58′-31°22′ N, 113°41′-115°05′ E, 709 m a.s.l.) is the capital of the Hubei Province and is located in the Jianghan Plain. The city lies at the confluence of the Yangtze and HanJiang rivers in central China. The Jianghan Plain is limited by mountain chains. The Tongbai-Dabie Mountain Range (500–800 m a.s.l.) lies to the north, the Wu and Daba Mountain Ranges (1500–2200 m a.s.l.) lie to the west, the Xuefeng Mountain Range (500–1500 m a.s.l.) lies to the south and the Luoxiao Mountain Range (900–1600 m a.s.l.) lies to the southeast.

According to the Köppen and Geiger (1936) climate classification, the study area has a humid subtropical climate and a differentiated four-season pattern with a marked monsoon effect, which begins in April and runs through August with the maximum precipitation occurring in June. The annual pattern is characterised by hot, humid summers (with an average of 29 °C and 80% rel. humidity in July), cool spring and autumn periods, and cold winters (4 °C, 70% rel. humidity with occasional snowfall (NMIC, 2022).

Wuhan is the sixth-largest Chinese city in terms of population. It has an area of 8494 km^2 and a population of 12.3 million people, with approximately 10.3 million residing in the urban area (Wuhan Council, 2021). This provincial capital is divided into three districts (Hankou, Hanyang and Wuchang) and is a key transport and communications point.

According to Querol et al. (2006), during the 2003–2004 period, in addition to major urban emissions from road traffic, construction/demolition and domestic and residential sources in a city of 9 million inhabitants, there were also important industrial emissions from the Changqian industrial estate. These emissions included steel production (Wuhan Steel Company, one of the largest steel companies in China), coke and iron alloy manufacturing, coal-fired power generation, petroleum chemical engineering, and smelting. The Environment Protection Bureau of Wuhan estimated that the emissions from these industrial activities accounted for 34% of secondary PM, 57% of primary PM and 45% of total SO_2 emissions in Wuhan. Coal combustion in this area accounted for up to 54% of total SO_2 emissions.

The long-range transport of dust from the Gobi and Taklamakan deserts and the Loess Plateau sporadically influence PM values in Wuhan, mostly during the spring-summer period (Ge et al., 2014); however, specific meteorological settings might favour these episodes in winter (Qian et al., 2004). Furthermore, southern and central China's air quality is also affected by the long-range and regional transport of PM emissions from widespread biomass burning in SE Asia (Liu et al., 2020).

3. Methodology

In the present study, we repeated the $PM_{2.5}$ sampling from June 2019 to January 2021, termed the second period (SP), on the campus of the China University of Geosciences (CUG) (urban background), very close to the Gaoxin monitoring site (the CUG is located 5 km north-northwest of Gaoxin). Notably, an intermediate COVID-19 lockdown period resulted in missing samples. The same analytical procedures were applied in the same laboratory to the 2019–2021 $PM_{2.5}$ samples to facilitate the comparison of major and trace $PM_{2.5}$ component concentrations and source contributions for Wuhan during the 2006–2007 and 2019–2021 periods.

3.1. Sampling

We performed 2 $PM_{2.5}$ sampling campaigns in Wuhan City. The $PM_{2.5}$ study conducted by Lv (2008) sampled and analysed approximately 50 major and trace elements, major soluble ions, and organic carbon (OC) and elemental carbon (EC) concentrations in 184 $PM_{2.5}$ 24-hr integrated samples. The sampling took place simultaneously from July 2006 to July 2007—defined as the first period (FP)—at the following three sites (Fig. 1):

- The Changqian industrial sampling site (114°25′38″E, 30°36′37″N, 38.5 m a.s.l.) was located northeast of Wuhan. Close to this site were industrial estates for the manufacturing of coke and iron alloy, a coal power plant, a petrochemical plant, a smelting plant and a thermal

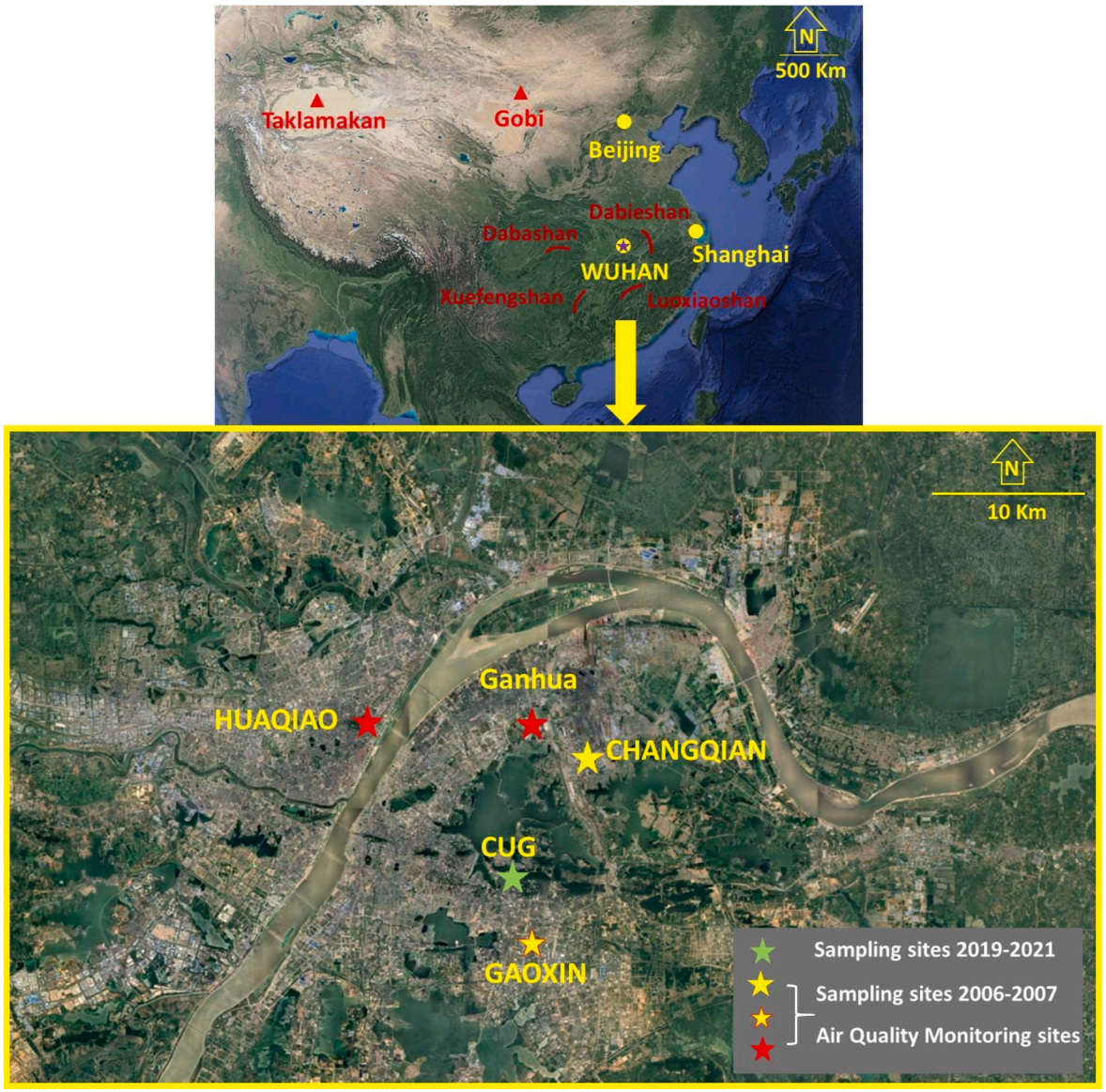

Fig. 1. Location of Wuhan and the 2006–2007 and 2019–2021 air quality monitoring and sampling sites.

steel rolling plant, among others. The Bureau of Environment Protection of Wuhan estimated that the emissions from these industrial activities accounted for 34% of secondary PM, 57% of primary dust and 45% of SO_2 emissions in the city.

- The Huaqiao urban background monitoring station (114°17′1″E, 30°37′11″N, 23 m a.s.l.) was located in the Hankou residential area in northern Wuhan on the terrace of a five-storey building. The distance to major busy roads was approximately 100 m. Consequently, major urban emissions close to the sampling site include road traffic as well as heating and cooking emissions.
- The urban-industrial air quality monitoring site of Gaoxin (114°23′33″E, 30°27′40″N, 47.6 m a.s.l.), located in a high-tech development zone of southern Wuhan on the terrace of a four-storey building. There were major busy roads at a distance of approximately 50 m. Additionally, many high-tech industries, such as electromechanical production, optical communication and medicine production, were located in this area. Consequently, major emissions close to the sampling site include road traffic and industrial emissions.

The number of samples collected at Changqian, Huaqiao and Gaoxin and subsequently analysed were 59, 58 and 47 $PM_{2.5}$ samples, respectively.

The second sampling campaign occurred from July 2019 to January 2021 at an urban background site located on the campus of the CUG in southern Wuhan (Fig. 1). This site is located on the terrace of a two-storey building (approximately 10 m a.g.l.) in the central part of the campus. The height of the CUG sampling site is equivalent to the ones from Changqian, Huaqiao and Gaoxin (in fourth to fifth floor terraces). All sites have an urban background pattern at this height. The environment is similar to that described for the Gaoxin site, which is located 5 km south-southeast of the CUG. In total, 81 $PM_{2.5}$ samples were collected at the CUG.

In both campaigns, 24 h $PM_{2.5}$ samples were collected using a high-volume sampler (Th–1000CII, Wuhan Tianhong Instrument Co., Ltd.) with a flow rate of 63 $m^3\ h^{-1}$ and equipped with a $PM_{2.5}$ impactor inlet using quartz microfiber filters with a 515 cm^2 area (QF20 Whatman and Schleicher & Schuell). The blank quartz filters were pre-heated at 450 °C for 4 h prior to use to eliminate organic interferences. By an error, the last 15 filters used were made of glass microfiber from the same brand, which did not allow determining the contents of a number of elements. These were excluded from the source apportionment analysis.

Due to the COVID-19 lockdown restrictions at the CUG occurring during the sampling campaign in 2019–2021, sampling was interrupted from 02/02/2020 to 05/12/2020. Furthermore, logistical issues prevented sampling from 07/16/2020 to 11/12/2020. Due to these missing sampling periods, only the months with samples for the 2019–2021 period (June–January, May–July and November–January) were selected from the 2006–2007 time series for comparison with the $PM_{2.5}$ concentrations, compositions, and source contributions from both campaigns.

Furthermore, daily data for SO_2, NO_2, $PM_{2.5}$, PM_{10} and CO were supplied for the three air quality monitoring sites (Huaqiao, Gaoxin and Ganghua; the latter was close to the Changqian site; Fig. 1) by the Wuhan Environmental Bureau.

By comparing the concentrations of pollutants measured at these three monitoring sites from June 2019 to January 2021, while excluding the aforementioned missing sample periods, very similar concentrations were obtained. The slight differences obtained between the averages from different sites and pollutants were only about 2–4% $PM_{2.5}$, 1–2% PM_{10}, 0–4% SO_2, <1% CO and 3–5% NO_2. Thus, we can consider the sampled $PM_{2.5}$ as representative of the entire sampling period.

3.2. Sample treatment and analysis

Before and after sampling, filters were weighted after equilibration for 48 h under stable temperature (20 °C) and relative humidity (50%) conditions and stored in aluminium foil at 4 °C before analyses. Once the mass was determined, the filters were cut into several sections for analysis. According to the methodology described by Querol et al. (2001), one-quarter of the filter was digested in a sequence of acids (HF: HNO_3:$HClO_4$) for the determination of major and trace elements via inductively coupled plasma mass spectrometry (ICPMS, iCAP-RQ, Thermo fisher Scientific, US) and inductively coupled plasma atomic emission spectrometry (ICP-AES, iCAP 6500 Radial View, Thermo Fisher Scientific). The NIST 1633b certified material was used in each digestion batch (1/4 of filter + 0.05 g of the NIST) to ensure the accuracy and precision as the error for each element is <10% except for P, Zr and Hf showing an error of 10–20%. Another quarter was leached for the extraction of water-soluble ions. Ammonium was analysed by using an ion-selective electrode (Thermo Scientific Model 710 +Thermo Orion), while SO_4^{2-}, Cl^- and NO_3^- were analysed by ion chromatography (IC, Dionex Aquion, Thermo Fisher Scientific, US). One punch (1.5 cm^2) from each filter was analysed using the thermal-optical transmittance carbon analyzer (Sunset Laboratory Inc., US) (based on Birch and Cary, 1996; Cavalli et al., 2010, for the 2006–2007 and 2019–2021 periods, respectively) to quantify EC and OC concentrations.

The following indirect determinations were obtained:

- The SiO_2 concentrations were estimated from Al_2O_3*2.5 according to Querol et al. (2001).
- The content of organic matter (OM) was obtained from OC*1.7 according to Rothenberg et al. (2014).
- The content of mineral matter (or crustal component) was determined by converting the mineral elements (Ca, Al, Fe, K, Mg, P, Ti) into the respective oxides (CaO, Al_2O_3, Fe_2O_3, K_2O, MgO, P_2O_5, TiO_2) and summing the concentration together with SiO_2.

3.3. Receptor modelling

Positive matrix factorisation (PMF) was used to identify the main sources of PM and estimate their daily source contributions. The US-EPA v.5 software was used. Equation (1) was used to solve the PMF model by expressing measured species concentrations as sums of different source contributions:

$$x_{ij} = \sum_{k=1}^{p} g_{ik} f_{kj} + e_{ij} \quad (1)$$

where the specified dataset is viewed as a data matrix X of i and j dimensions, where i is the number of samples and j is the measured chemical species with its uncertainties, u. p stands for the number of factors, f stands for the species concentration in each source, g stands for the source contribution of each factor to each species and e_{ij} stands for the residual of each sample/species (Paatero, 1997; Paatero and Tapper, 1994). PMF imposes non-negativity constraints on the f and g factors and uses individual data uncertainty estimated following the method of Amato et al. (2009). As input for PMF, the species selection was based on the signal-to-noise (S/N) method (Paatero and Hopke, 2003). PMF diagnostics were estimated by means of the EPA PMF5 software using the displacement (DISP) analysis method, which includes the sensitivity of the solution to small changes and the effects of rotational ambiguity (Paatero et al., 2014). Since this study aimed to compare source contributions among different periods, we included both campaigns in the same input dataset, thereby merging a total of 245 valid daily $PM_{2.5}$ samples for analysis. For both campaigns, the same number of species and analytical methods were used. Although the chemical profiles of emission sources might have changed from one campaign to another, we merged the two datasets to have greater statistical power and for better comparability of the source contributions between the two campaigns.

3.4. Air mass back-trajectories

To support data interpretation on the influence of mineral desert dust transport from the Taklamakan or Gobi deserts, air mass back-trajectories were calculated at receptor heights of 750, 1500 and 2500 m a.s.l. for each sampling day at 12 UTC using GDAS meteorological data and by modelling vertical velocity for central Wuhan using the Hybrid Single-Particle Lagrangian Integrated Trajectory (HYSPLIT) model from the National Oceanic and Atmospheric Administration (NOAA, USA) (Stein et al., 2015). The high altitude of the receptor heights was selected to detect the possible long-range transport of dust, which usually occurs at high altitudes.

3.5. Evaluation of $PM_{2.5}$ inter-annual trends with meteorological correction

The *Chinese Meteorological Industry Standard QX/T479* (2019) was used for analysing actual $PM_{2.5}$ trends, as well as those after the annual correction of the meteorological effects, and accordingly describing trends attributable to decreases or increases of emissions of primary PM and the precursors of secondary PM. This value is defined as the meteorological condition assessment index or the environmental meteorology index (EMI). This comprehensively considers the multiple dynamic mechanisms of the influence of meteorological conditions on $PM_{2.5}$ concentrations, including sedimentation, transmission and diffusion. It is calculated by the numerical CUACE model of the China Meteorological Administration (Zhou et al., 2012). In this study, the national daily EMI data from 2013 to 2021 were used to extract the EMI values of nine state-controlled air quality monitoring stations in Wuhan, the arithmetic average of which was taken as the daily EMI value of Wuhan. The annual variation of EMI in Wuhan was analysed, and the changes in the contributions of meteorological conditions and emission reduction measures over the years were evaluated. A negative value indicates that the meteorological conditions were good and reduced the concentration of fine particles, while a positive value indicates poor meteorological conditions where $PM_{2.5}$ increased. Alternatively, for the changes due to variations in emissions, a negative value indicates an emissions reduction, while a positive value indicates an emissions increase.

4. Results and discussion

4.1. Review of emission sources of air pollutants and trends in Wuhan

To support further interpretations of the results, a review of the emission patterns of Wuhan City and Hubei province was performed to compare the two study periods.

According to Zhou et al.'s (2018) study of Wuhan, in 2014, fuel combustion sources dominated the contributions to SO_2 emissions (64% of 102,699 t), mobile sources dominated the contributions to NOx emissions (51% of 170,197 t) and fugitive dust and industrial production accounted for the largest contributions to PM_{10} and $PM_{2.5}$ primary emissions (162,818 and 71,263 t, respectively). Industrial production and road traffic also accounted for most of the volatile organic compound (VOC) emissions (197,996 t). Black carbon and OC emissions were mainly attributed to mobile sources and biomass burning. Finally, NH_3 emissions (16,187 t) were mainly associated to agricultural sources. The highest air pollutant emissions were typically from the Qingshan and Xinzhou administrative regions. Ferrous metal smelting and processing was the primary source of SO_2 (28%), $PM_{2.5}$ (40%) and PM_{10} (23%).

According to the Wuhan Ecological Environment Bureau (WEEB, 2021), at the end of 2017, there were 9230 industrial sources, 1655 large-scale livestock and poultry farms, 2673 domestic sources and 999 centralised pollution-controlled facilities in Wuhan. The top five industries included 1282 metal plants, 1241 non-metallic mineral plants, 884 textile and garment factories, 588 general equipment-manufacturing factories, and 558 rubber and plastic factories. In 2017, the industrial sector comprised 122 desulphurisation facilities, 89 de-NOx facilities and 2881 dust removal facilities. The 2017 emissions (WEEB, 2021) were drastically lower when compared to 2014 (Zhou et al., 2018), with a 64% reduction in SO_2, 42% reduction in NOx and 66% reduction in PM_{10}. In 2017, industrial emissions accounted for 38, 40, 56 and 45% of Wuhan's total SO_2, NOx, PM_{10} and VOC emissions, respectively, while mobile sources accounted for <1, 60, 2 and 27% and domestic sources accounted for 62, <1, 41 and 28%, respectively (WEEB, 2021). Thus, industrial sources' contributions to SO_2 emissions were reduced from 64 to 38% between 2014 and 2017, with a major domestic contribution (62%) in 2017. Conversely, the increased NOx contribution from mobile sources ranged from 51 to 60%. PM_{10} emissions in 2017 were driven by industrial and domestic sources (56 and 41%, respectively), while those for VOCs were driven by industrial, mobile and domestic sources (46, 27 and 28%, respectively). Qin et al. (2020) reported that in 2006, NH_3 emissions in Hubei Province (for which Wuhan is the capital) totalled 371,000 t, while in 2016 these emissions were 475,000 t. In addition to this 26% increase in NH_3 emissions from 2006 to 2016, there were slight changes in the major contributions in 2016, with 72, 16, 4, 3 and 5% of Hubei's NH_3 being emitted by livestock, fertilisation, human excreta, industry and all the other sources, respectively, while the 2007 emissions were 69, 18, 7, 2, and 5%, respectively. However, based on the same emission inventory for Wuhan City, Zhang et al. (2022) reported a rather different source contribution to NH_3 emissions for 2015 when compared to the one for Hubei Province, with industry (58%), livestock (14%), fertilisers, waste disposal (7%) and road traffic (5%) being the major sources.

The ferrous metal smelting and rolling processes, the non-metallic mineral products industry and the non-metallic mining and dressing industry accounted for 80% of SO_2 industrial emissions in 2017. The ferrous metal smelting and rolling industry, power and heat production and supply industry, and the non-metallic mineral products industry accounted for 87% of the industrial NOx emissions. The non-metallic mineral product industry, ferrous metal smelting and rolling industry, and metal product industry accounted for 69% of the PM_{10} emissions from industrial sources. The oil, coal and other fuel processing industries, chemical raw materials and chemical product manufacturing industries, and the automobile manufacturing industry accounted for 63% of the total VOC emissions from industrial sources.

4.2. $PM_{2.5}$ concentrations

The reduction rates of $PM_{2.5}$, SO_2, and NO_2 may not be linear in some cases, but, for simplicity, comparation of data for 2006–2007 and 2019-2021 and the average decrease per year are provided. Average $PM_{2.5}$ concentrations for the study periods were 129, 116 and 117 μg m^{-3} for Gaoxin, Huaqiao and Changqian, respectively, in the FP and 52 μg m^{-3} for the CUG site in the SP. This value represents a 60% reduction when compared to Gaoxin (the closest location to the CUG; 5 km south-southeast) and a 57% reduction compared to the average of the three sites. When considering the 2006–2007 data from the three air quality monitoring stations (Fig. 1) of the Wuhan Environmental Bureau (Lv, 2008), the averaged concentrations ranged from 114 to 130 for $PM_{2.5}$, 62 to 82 for SO_2 and 51–54 μg m^{-3}; in the 2019–2021 period, the values were 39–47 and 8–9 μg m^{-3}, respectively. This accounts for an average $PM_{2.5}$ decrease of 65% with a reduction rate (without meteorological correction) of −4.7 μg m^{-3} yr^{-1} during the 2007–2021 period. For SO_2, the decrease was 88% at a rate of −6.3 μg m^{-3} yr^{-1}. For NO_2, the reduction was only 25% (1.8 μg m^{-3} yr^{-1}). During the 2013–2018 period, Zhai et al. (2019) reported a general decrease in annual mean $PM_{2.5}$ across China of 30–50%, with a reduction rate of −5.2 and −4.6 μg m^{-3} yr^{-1}, without and with meteorology correction, respectively. For SO_2 and NO_2, they found average decreases of 67 and 13%, respectively, during the 2013–2017 period.

Taking the meteorological conditions and $PM_{2.5}$ concentrations in 2013 as a baseline in this study, the contributions of meteorological conditions and emission reduction measures to the reduction of $PM_{2.5}$ concentrations were evaluated for the 2014–2021 period using the EMI approach. For the 8-year period, annual average $PM_{2.5}$ concentrations in Wuhan decreased by approximately 55% when compared to those of 2013 after meteorological correction (Table 1), with a meteorology-corrected decrease of −6.9 μg m^{-3} yr^{-1}. However, it seems that during the SP, the decrease of $PM_{2.5}$ attributable to the abatement of emissions ended since values remained constant. These results are important because the COVID-19 lockdown accounted for relevant reductions in emissions of PM and gaseous precursors. However, this effect was likely counteracted by the increase of emissions after the lockdown to recover production and because most of the $PM_{2.5}$ was from a secondary origin. Several studies on the effect of the COVID-19 lockdown's impact on air quality reported drastic decreases in primary pollutants (e.g., NO and NO_2) but very smooth effects in $PM_{2.5}$ concentrations due to atmospheric conditions favouring the formation of secondary pollutants ($PM_{2.5}$ and O_3) (Silver et al., 2020).

According to these results and the previously reported emissions trends, it is clear that both $PM_{2.5}$ and SO_2 dramatically decreased from 2006 to 2021 due to emission reductions of primary PM and SO_2, while the decrease of NO_2 was much less pronounced.

Table 1
Annual percentage of $PM_{2.5}$ concentration variation compared to 2013 caused by changes in meteorological conditions and emission reduction measures in Wuhan.

Year	$PM_{2.5}$ concentration	Due to meteorology	Due to emissions abatement
2014	−14.4	6.2	−20.6
2015	−25.5	3.3	−28.8
2016	−39.5	1.8	−41.3
2017	−44.0	3.0	−47.0
2018	−48.7	1.6	−50.3
2019	−51.7	4.7	−56.4
2020	−60.1	−5.9	−54.2
2021	−59.6	−4.5	−55.1

4.3. $PM_{2.5}$ composition differences

Table S1 and Fig. 2 summarise the different $PM_{2.5}$ component concentrations measured at the CUG during the SP, as well as those at the three sampling sites during the FP. Upon comparing the SP CUG data with the closest site in the FP (Gaoxin), it is evident that NH_4^+, mineral species, $PM_{2.5}$, EC, OM, Na, Cl^-, SO_4^{2-} and the remaining fraction that could not be identified were reduced by 48, 55, 60, 63, 65, 68, 71, and 60%, respectively, while NO_3^- only declined by 22%. Thus, average SO_4^{2-} concentrations decreased more rapidly than $PM_{2.5}$, while NO_3^- and NH_4^+ declined less rapidly than bulk $PM_{2.5}$. In terms of major changes in the relative contributions to $PM_{2.5}$, SO_4^{2-} and other PM species contributions were reduced by 6 and 3%, respectively, while NO_3^- and NH_4^+ increased by 8 and 3%, respectively (Fig. 2).

The higher decrease of SO_4^{2-} than $PM_{2.5}$ is probably due to the drastic reduction SO_2 (mostly due to reduction of coal combustion and the implementation of desulphurisation controls), the precursor SO_4^{2-}. Furthermore, NO_3^- levels decreased less than most of other $PM_{2.5}$ components (probably due to the lower reduction of NOx and NH_3 emissions) and so this diminished the reduction of $PM_{2.5}$ ($PM_{2.5}$ 48% while SO_4^{2-} 60%).

Table S2 summarises the average concentrations of the 2006–2007 and 2019–2021 measurement campaigns for major soluble ions, OC, EC and multiple trace elements, as well as those reported by prior studies conducted in Wuhan. The trend analysis of these data shows that OC and SO_4^{2-} exhibited the largest reductions, with rates of −0.93 and −0.89 μg m^{-3} yr^{-1}, respectively (R^2 = 0.84 and 0.70, respectively; −3.7 and −3.9% yr^{-1}, respectively), followed by NH_4^+, EC and Cl^- at −0.29, −0.22 and −0.09 μg m^{-3} yr^{-1}, respectively (R^2 = 0.70, 0.70 and 0.73, respectively; −2.7, −4.1 and −3.9% yr^{-1}, respectively). However, NO_3^- did not show a significant decrease (R^2 = 0.08).

The following groups of major and trace elements can be identified according to the decreases in concentrations from the 2006–2007 to 2019–2021 periods:

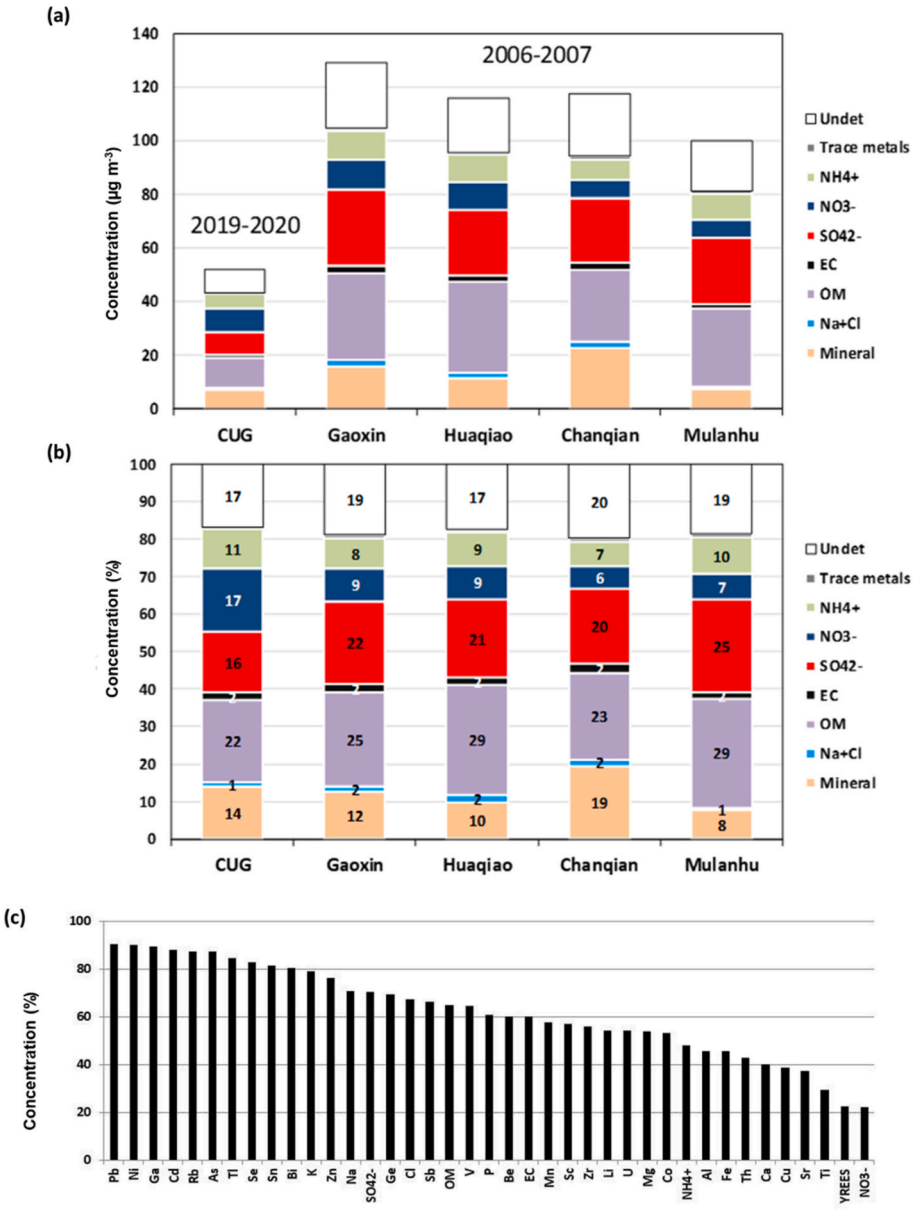

Fig. 2. a) Concentrations and b) percentage contributions of major $PM_{2.5}$ components measured at the CUG during the 2019–2021 period and those of the three sampling sites during the 2006–2007 period. c) Decrease in percentage, of the concentrations of major and trace elements during the SP when compared to the FP.

- -90 to −76%: Pb, Ni, Ga, Rb, As, Tl, Se, Sn, Bi, K and Zn; most of these typically originate from coal combustion (Pacyna et al., 1985).
- -71 to −57%: Na, Ge, Sb, V, P, Be, Mn and Sc; most of these also largely originate from coal combustion, but with relevant contributions from dust resuspension, road traffic and construction (Amato et al., 2016; Senior et al., 2020 and references therein).
- -54 to −22%: Li, U, Mg, Co, Al, Fe, Th, Ca, Cu, Sr, Ti and Y, as well as rare earth elements (YREEs); mostly from dust resuspension and road traffic and construction (Soba et al., 2022). NO_3^- mostly arising from NOx from traffic in current environmental scenarios, experienced a 22% reduction.

The reduction of coal-related elements is probably due to a combination of the implementation of stricter emission controls, reduction of coal utilization in power generation and industry, and the closure of old industrial units and the moving of these to external parts of the city with a higher efficiency and environmental standards. All this occurring between FP and SP.

Taking the data from Table S2, the following annual reduction rates were obtained for the most potentially hazardous elements: Zn −19.4 ng (5.8%) m^{-3} yr^{-1}; Pb −23 ng (6.9%) m^{-3} yr^{-1}; As −2.7 ng (6.5%) m^{-3} yr^{-1}; Ni −1.0 ng (6.6%) m^{-3} yr^{-1}; Cd −0.4 ng (6.7%) m^{-3} yr^{-1}; Sn −0.9 ng (6.1%) m^{-3} yr^{-1}; Sb −0.4 ng (5.3%) m^{-3} yr^{-1}; K −0.2 μg (6%) m^{-3} yr^{-1}; Ca −0.03 μg (3.2%) m^{-3} yr^{-1}; Cu −0.8 ng (3.1%) m^{-3} yr^{-1}; Fe −0.09 μg (4.4%) m^{-3} yr^{-1}.

Thus, it seems that the highest reductions were observed for the coal combustion and smelting-related elements, while those partially emitted by vehicle wear (Fe, Cu, Sb, Sn from vehicle brakes), construction and demolition (Ca), and biomass burning (fine K) (Amato et al., 2016) exhibited the lowest reductions.

4.4. $PM_{2.5}$ ion balances

NO_3^- and SO_4^{2-} are formed in the atmosphere from NOx and SO_2, respectively. Coal combustion has been the primary source of SO_2 in the study area, while NOx is emitted by a mix of high-temperature combustion sources, including road traffic (Lv, 2008). In the 2019–2021 sampling campaign, the $[NO_3^-]/[SO_4^{2-}]$ ratio ranged from 0.01 to 2.42, with an average value of 0.75. However, during the FP in Gaoxin, Changqian and Huaqiao, this ratio ranged from 0.02 to 0.77 (mean 0.31), 0.01 to 0.66 (0.23) and 0.02 to 0.85 (0.33), respectively. The air quality policy actions implemented since 2013 resulted in an 88% mean decrease in SO_2 at the three air quality monitoring stations, which is mostly attributable to the decrease of the emissions from coal combustion attributed to the improvements reported above. Alternatively, the NO_2 reduction was only 25%. This smaller decrease in NO_2 is likely attributable to the effect of the same policies but was partly undermined by increases in Wuhan's vehicle fleet. According to WEEB (2021), the number of vehicles in Wuhan reached 2.6 million by 2017, representing a 3.7-fold increase when compared to the 0.71 million that were present in 2006 (Lv, 2008).

The ion balance scatter plot (Fig. 3) shows that in 2006–2007, there was an excess of +12% of SO_4^{2-} versus NH_4^+ at Changqian, suggesting the occurrence of acidic H_2SO_4/NH_4HSO_4 close to the large coal-burning industrial sources at that time. However, at Huaqiao and Gaoxin, which are both influenced by traffic exhaust, deficits of −17 and −5% SO_4^{2-} versus NH_4^+ were observed, respectively. However, this excess NH_4^+ was neutralised by NO_3^-. Thus, only 5% of NH_4^+ occurred as NH_4NO_3 and 95% occurred as $(NH_4)_2SO_4$ in the $PM_{2.5}$ of Gaoxin in the FP. These proportions were markedly different in the CUG during the SP, where 55% of NH_4^+ was present as NH_4NO_3 and only 45% was present as $(NH_4)_2SO_4$. Therefore, the dominant chemical forms of SO_4^{2-} were $(NH_4)_2SO_4$ in 2006–2007 and NH_4NO_3 during the 2019–2021 period.

The marine aerosol contribution to the atmospheric aerosol is typically associated with Cl^- and Na^+ due to their major marine origin; however, their contributions are more relevant to PM_{10} than to $PM_{2.5}$. The typical marine mass Na^+/Cl^- ratio is close to 0.56, while the ratio observed in Gaoxin in 2006–2007 was 0.24 (Fig. 4). Thus, a high Cl^- excess is evidenced with respect to the marine ratio, indicating a major anthropogenic origin of Cl^- in Wuhan (as it can be also expected from its inland-continental location. Furthermore, mineral dust, and coal and biomass burning can be relevant sources of Na. The marked Na decrease (73% Na^+ $PM_{2.5}$ at the CUG during the SP compared to Gaoxin in the FP) points also to a major anthropogenic origin. The prevalent coal combustion origin of Cl^- in northern China (occurring mostly as NH_4Cl) has been well supported by several studies, such as those of Li et al.(2019a,

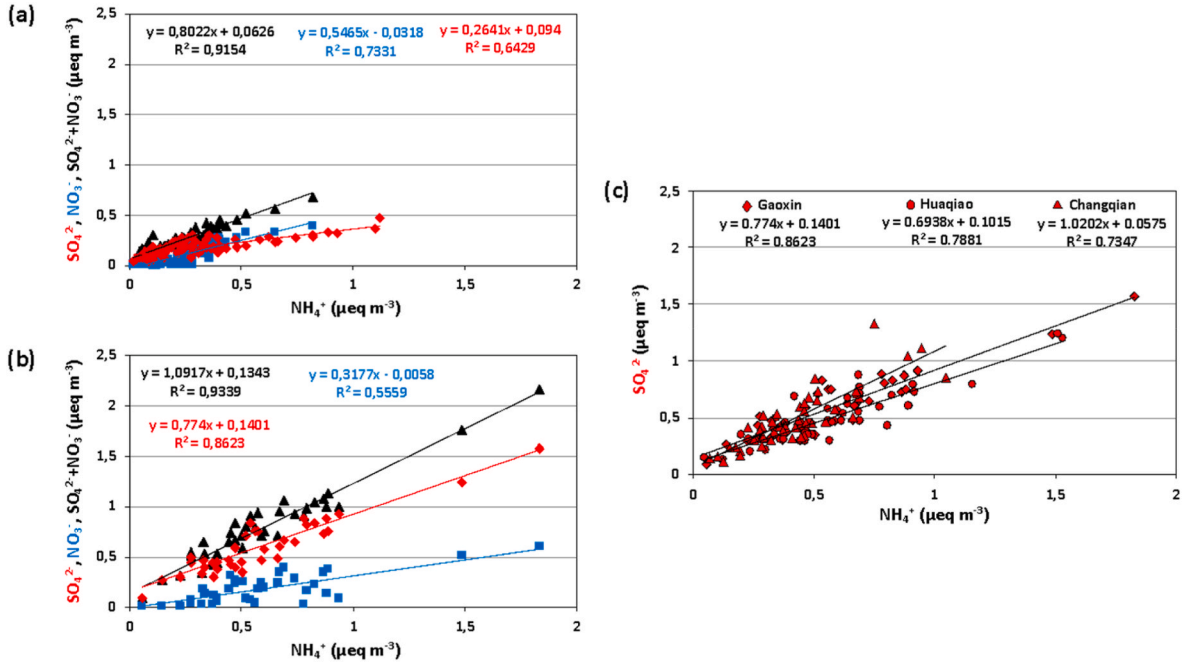

Fig. 3. Ion balance of SO_4^{2-}, NO_3^- and $SO_4^{2-} + NO_3^-$ with NH_4^+ at the CUG during the 2019–2021 period (a) and at Gaoxin in 2006–2007 (b). Ion balance comparison of SO_4^{2-} with NH_4^+ at Gaoxin, Huaqiao and Changqian in 2006–2007 (c).

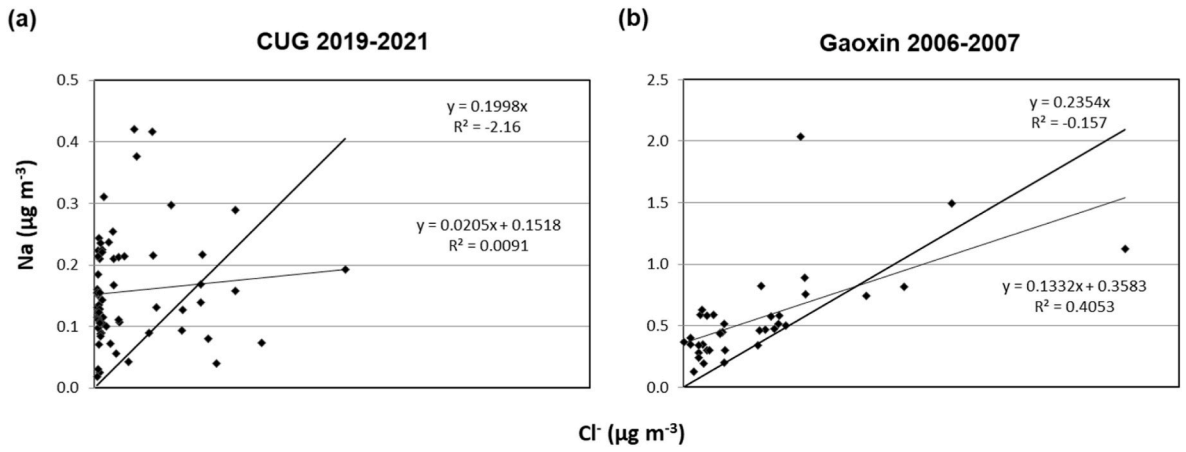

Fig. 4. Na^+/Cl^- scatterplots a) CUG during the SP and b) Gaoxin in the FP, showing a Na^+/Cl^- ratio much lower than 0.56 (the typical marine ratio). This, together with the marked decrease of Na^+, points to a major anthropogenic origin of Na in the SP.

b), Yu et al. (2013) and Zíková et al. (2016). Furthermore, the high correlation of Na^+/NO_3^- in 2006–2007 points also to an aged sea salt. In the CUG during the SP, the Na^+/Cl^- and Na^+/NO_3^- correlations were lost. Nevertheless, a NO_3^-/Cl^- correlation was observed (similarly to Gaoxin in the FP), also pointing to a major anthropogenic source of Cl^-. Consequently, Na arises from aged sea salt and Cl^- is probably a secondary inorganic (SIC) compound in this case. Brewer and Shirrow (1975), as well as Qin (1995), showed that Cl^- might be derived from coal combustion when ratios lower than the marine Na^+/Cl^- ratios were measured.

4.5. $PM_{2.5}$ source apportionment

For the PMF source apportionment analysis, different solutions with varying numbers of factors were explored. As diagnostic criteria, we used the Q values ($Q_{robust}/Q_{theoretical}$), distribution of scaled residuals, G space plots, interpretability of the factor profiles and reasonableness of the source contribution seasonality. As a result, for the FP, a nine-factor solution was selected as the most reliable using the following species as 'strong': OC, EC, Al, Ca, Fe, K, Mg, Na, SO_4^{2-}, NO_3^-, NH_4^+, Cl^-, P, Ti, V, Mn, Co, Cu, Zn, As, Rb, Cd, Sn, Sb, Cs, La, Ce, Pb and Bi. The following species were classified as 'weak': Cr, Se, Sr, Ba, Gd and Tl. Notably, Li, Be, Sc, Ni, Ga, Ge, Y, Nb, Ta, W, Th and U were not used (Table S3a). An extra uncertainty of 15% was applied. Alternatively, for SP, a five-factor solution was identified as the most suitable. In this case, the strong species were: OC, Al, Ca, Fe, K, Mg, Na, SO_4^{2-}, NO_3^-, NH_4^+, Cl^-, P, Ti, V, Mn, Co, Cu, Zn, Ga, As, Se, Rb, Sr, Cd, Sn, Sb, Cs, Ba, La, Ce, W, Tl, Pb and Bi; whilst, EC, Cr and Ni were classified as weak. Furthermore, Li, Be, Sc, Ge, Y, Nb, Gd, Ta, Th and U were bad species, not used (Table S3b). An extra modelling uncertainty of 10% was applied. The variable $PM_{2.5}$ was considered a total and also a weak variable. These solutions were selected based on the DISP and BS diagnostics which show high robustness for both period PMF analyses as all profiles are mapped by 93–100%, except for two factors (77% for the SP and 84% for the FP) (Table S4). A few samples were excluded from the PMF since some coincided with Chinese New Year fireworks displays (02/17/2007, 01/24/2020) and the Chinese Spring Festival (05/14/2007, 05/21/2020). Also, the last samples of 2020 were excluded from the SP PMF study as, by a sampling error, glass microfiber filters were used, which did not allow determining the contents of a number of elements.

The source profiles identified by the PMF analysis are shown in Fig. 5. The temporal series of each source contribution to $PM_{2.5}$ and DISP are displayed in Fig. 6, and the average source apportionment at each sampling site is presented in Fig. 7. There were no factor swaps reported for the allowed dQmax examined by the model (fixed at 4, 8, 15 and 25 in this study). Bootstrap (BS) runs, which involved mapping the BS factor to the base factor suiting the highest correlation, did show a high correlation with the base run. Complete diagnostics for the PMF analyses (bootstrap and displacement) are provided in the Supplemental Material Table S4. Below, it is described the common and distinct factors found for the FP and SP. Four out of five profiles from the SP PMF study coincide with the ones in the FP PMF analysis. Firstly, find the SP factors, ordered by the average source contribution and compared with FP data and, secondly, the remaining non-common factors.

4.5.1. Secondary nitrate

This factor, secondary nitrate (SECN), is the first profile (31% contribution to $PM_{2.5}$) for SP and the second (22% contribution to $PM_{2.5}$) for the FP. It is characterised by high contributions, to the factor composition, of NO_3^-, NH_4^+, and SO_4^{2-}, thus, 34%, 14% and 10% stands for the SP and 36%, 12% and 14%, for the FP, respectively. It also shows a clear seasonality and high winter-autumn and low summer contributions typical of ammonium nitrate (due to its thermal instability under typical summer temperatures) (Harrison and Pio, 1983). This factor accounted for the high explained variation of NO_3^- (83%), followed by Cl^- (79%), NH_4^+ (48%), OC (24%) and SO_4^{2-} (20%), in the SP, whilst for the FP explained the variation of NO_3^- (76%), NH_4^+ (27%) and Cl^- (24%). The NO_3^-/NH_4^+ ratio equals 2.4 and 2.9, in the SP and FP, respectively. DISP results, which highlight the uncertainty generated by the amount of rotational space, indicate high robustness due to the small intervals for the main tracers; however, other elements present higher variability. Indeed, SECN (with smaller proportions of secondary organic aerosols, sulphate and chloride) was largely generated in the FP from the high coal-combustion and industrial NOx emissions, while this was highly influenced by NOx from traffic in the SP. This source contributed 22% (27 μg m^{-3}) and 11–19% (12–23 μg m^{-3}) in the FP for Gaoxin and the other two sites, Changqian and Huaqiao, respectively, while contributing 31% (14 μg m^{-3}) at the CUG site during the SP. Thus, this contribution decreased by 48% (13 μg m^{-3}) from the FP to the CUG in the SP.

4.5.2. Mineral, road and desert dust

This second factor, mineral, road and desert dust (MRDD), is the second profile (30% contribution to $PM_{2.5}$) for SP and the sixth (6% contribution to $PM_{2.5}$) for the FP. It is characterised by high contributions (SP%, FP%) of OC (15%, 15%), SO_4^{2-} (6%, 14%), NO_3^- (4%, 6%) and Ca, Al, and K (3%, 2–6%). It highly contributed to the explained variation of Al (85%, 40%), Mg (85%, 52%), Ti (81%, 43%), Ca (80%, 62%), Sr (78%, 24%), Ba (69%, 13%), La (64%, 21%) and Ce (60%, 30%), for the SP and FP, respectively. There are very small DISP intervals for the main tracers and larger intervals for OC, EC, NH_4^+ and Cl^- that can rise to higher concentrations than the base run profile. There is

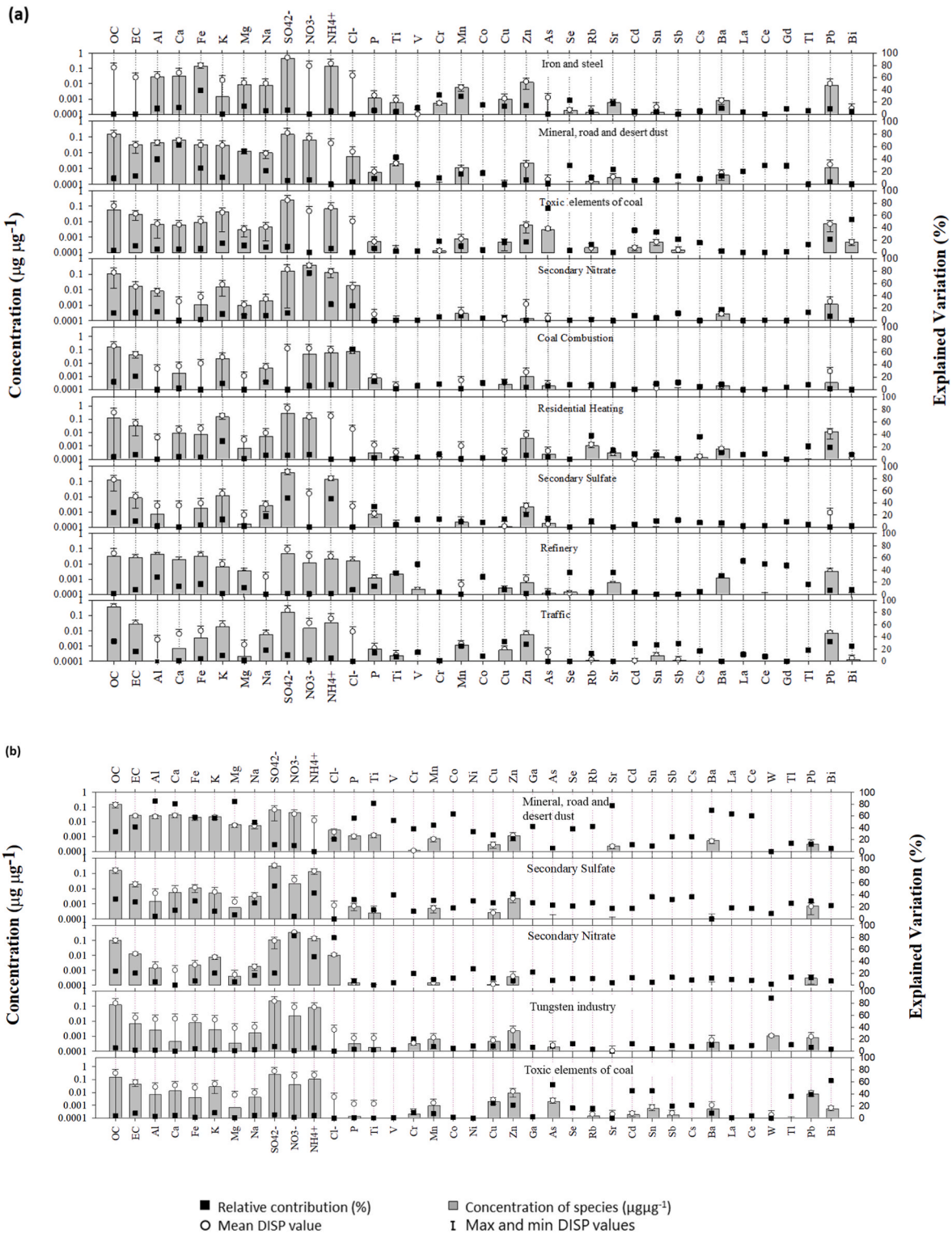

Fig. 5. Chemical profiles of the PMF analysis applied to inorganic $PM_{2.5}$ speciation datasets
From a) Changqian (industrial), Huaqiao (urban) and Gaoxin (industrial-urban) in 2006–2007 (160 samples, 29 species) and from b) CUG during the 2019–2021 period (urban) (66 samples, 35 species). PM components are shown on the x-axis.

also a greater variability for Fe, SO_4^{2-} and NO_3^-; however, the factor stability is not affected. The factor profile is clearly a mineral one, which is enriched in Ca and associated with dust (Amato et al., 2016). The Ce/La ratio is 1.7 (SP) and 2.7 (FP), close to the Earth's crust average ratio of 1.7 (Haynes, W.M., Lide, D.R., 2017). Source contributions do not show a clear seasonal pattern and are characterised by random concentration peaks at all sites, which was likely due to multiple construction activities or dust resuspension. Sporadically, RD peak contributions also include those from desert dust (mostly from the Taklamakan Desert followed by the Gobi Desert), as supported by the results of the back-trajectory analysis (Figure S1). This source contributed 6% (8 μg m^{-3}) and 14–6% (16–7 μg m^{-3}) of the $PM_{2.5}$ for Gaoxin,

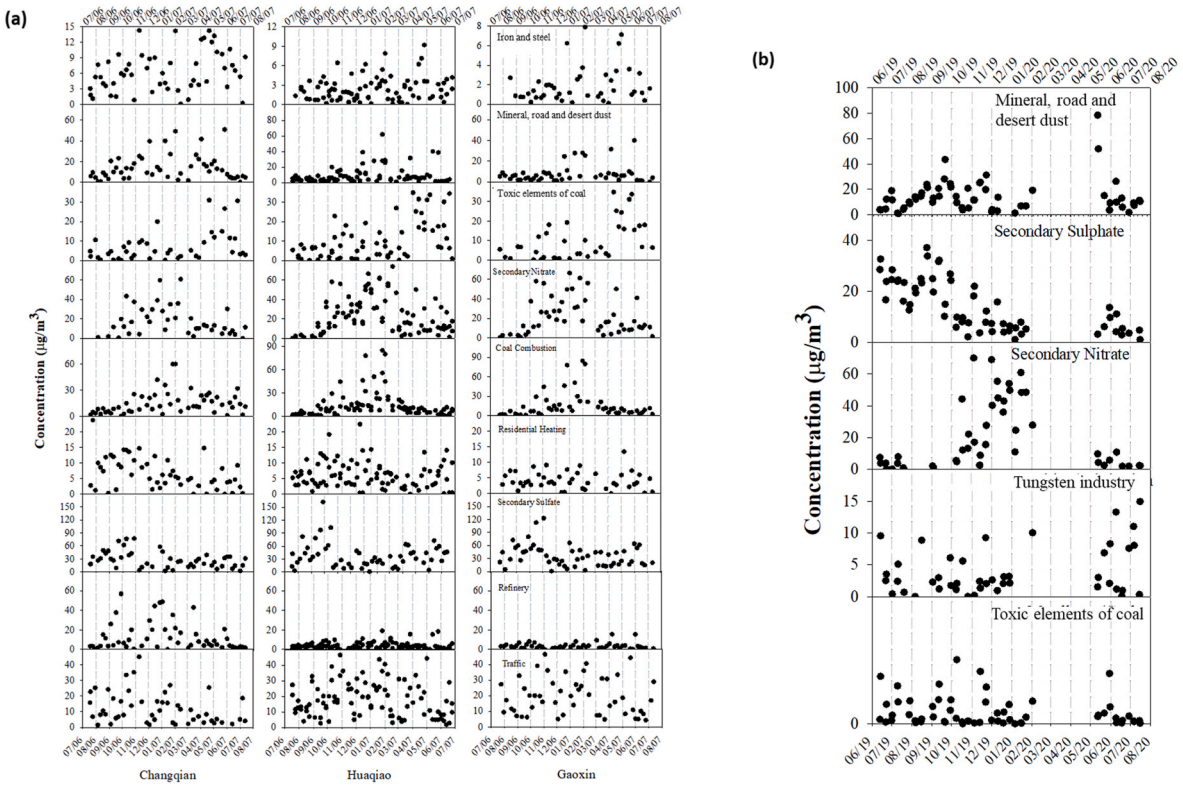

Fig. 6. Seasonal evolution of the contribution of main pollution sources identified at Wuhan (a: 2006–2007 and b: 2019–2021) by PMF analysis applied to inorganic $PM_{2.5}$ speciation datasets.

Changqian and Huaqiao, respectively, while it contributed 30% (13 μg m^{-3}) at the CUG sitevd during the SP. Thus, this contribution increased by 62,5% (5 μg m^{-3}) from the FP to the SP.

4.5.3. Secondary sulphate (and partially secondary organics)

The third factor for the SP, secondary sulphate (SECS), contributes 29% to the $PM_{2.5}$, while this fits the first factor of the FP, contributing 29% to the $PM_{2.5}$ composition. This profile is characterised by a factor composition rich in SO_4^{2-} (30%, 36%), OC (15%, 12%) and NH_4^+ (13%, 14%), for the SP and FP, respectively. It highly contributes to the explained variation of SO_4^{2-} (55%, 48%), NH_4^+ (43%, 47%), Zn (41%, 21%), V (40%, 13%), Cs (37%. 8%), Sn (36%, 10%), OC (33%, 24%), Sb (32%, 12%) and P (32%, 34%). The SO_4^{2-}/NH_4^+ ratio reached 2.3 and 2.6, in the SP and FP, respectively. Moreover, the DISP results show very small DISP intervals for the main tracers, indicating the high robustness of this factor. Instead, higher variabilities in NO_3^-, EC and Fe, among others, are observed; however, they did not affect the stability of this factor. Thus, this source contribution is interpreted as secondary ammonium sulphate, with a contribution of secondary organic aerosol (given the extremely high OC/EC, as well as the OC contribution). Some contributions from coal (SO_4^{2-}, Zn), metallurgy (Fe) and oil (SO_4^{2-}, V) combustion are likely present in this source (Arruti et al., 2011; Kim and Hopke, 2008; Li et al., 2020; Song et al., 2008). In the FP, emissions from typical stoves burning lump coal or briquettes will also produce significant quantities of primary sulphate and primary oxidised OC (Dai et al., 2019; Li et al., 2019a). This factor shows the typical regional sulphate seasonality with high summer levels and isolated autumn-winter peaks attributable to anticyclonic episodes (Meng et al., 2017). This source is estimated to contribute 29% (36 μg m^{-3}) of the $PM_{2.5}$ at Gaoxin and 21–31% (24–36 μg m^{-3}) at Changqian and Huaqiao in the FP, while it contributed 29% (13 μg m^{-3}) at the CUG during the SP. Thus, this source contribution decreased by 64% (23 μg m^{-3}) from the FP at Gaoxin to the SP at the CUG site.

4.5.4. Tungsten industry

The fourth profile for the SP, contributing 6% to the $PM_{2.5}$ composition is named tungsten industry (W). This factor is identified in the SP PMF analysis, not in the FP. This is characterised by high contributions to the factor composition of SO_4^{2-} (22%), OC (12%) and NH_4^+ (8%). This factor accounted for the high explained variation of W (89%), followed by Cr (20%) and Se and Cd (13%). DISP swaps and BS matching base run results show this factor is well mapped and has highly robustness. The W alloy company do not use recycled materials so they are smelting the W and this is likely the reason for the unique factor. This source is estimated to contribute 6% (3 μg m^{-3}) of the $PM_{2.5}$ the CUG site.

4.5.5. Toxic elements of coal and industry

The fifth-SP factor is named toxic elements of coal (TEC), contributing a 4% to the FP $PM_{2.5}$ composition and it is the fourth profile in the FP. This is characterised by a profile with high contributions of SO_4^{2-} (24%, 25%), OC (14%, 6%), NH_4^+ (10%, 7%) and EC (4%, 3%), for the SP and FP, respectively. This profile highly contributes to the explained variation (SP%/FP%) of Bi (62%, 53%), As (55%, 71%), Cd (45%, 36%), Sn (45%, 33%), Pb (39%, 21%), Tl (36%, 13%) and Cu (24%, 17%). Based on the DISP results, very small DISP intervals are observed for the main tracers, indicating the high robustness of this factor. This profile reveals coal consumption and industrial production as the main toxic heavy metal emission sources, showing high levels of As, Pb and Cd, among others (Cheng et al., 2014). High As levels are also typically found in industrial emissions related to smelting or other metal-based industries (Arruti et al., 2011). These typical traces of metallurgy emissions agree with prior PM_{10} speciation studies conducted in Wuhan in 2003–2004 by Querol et al. (2006). This contribution has no clear seasonal pattern and is characterised by sporadic concentration peaks, which are typical of industrial areas. This source contributed 10% (12 μg m^{-3}) and 6–7% (7–8 μg m^{-3}) at Gaoxin and the other two sites in the FP, respectively, while contributing 4% (2 μg m^{-3}) at the CUG site during the SP. Thus, this contribution decreased in absolute

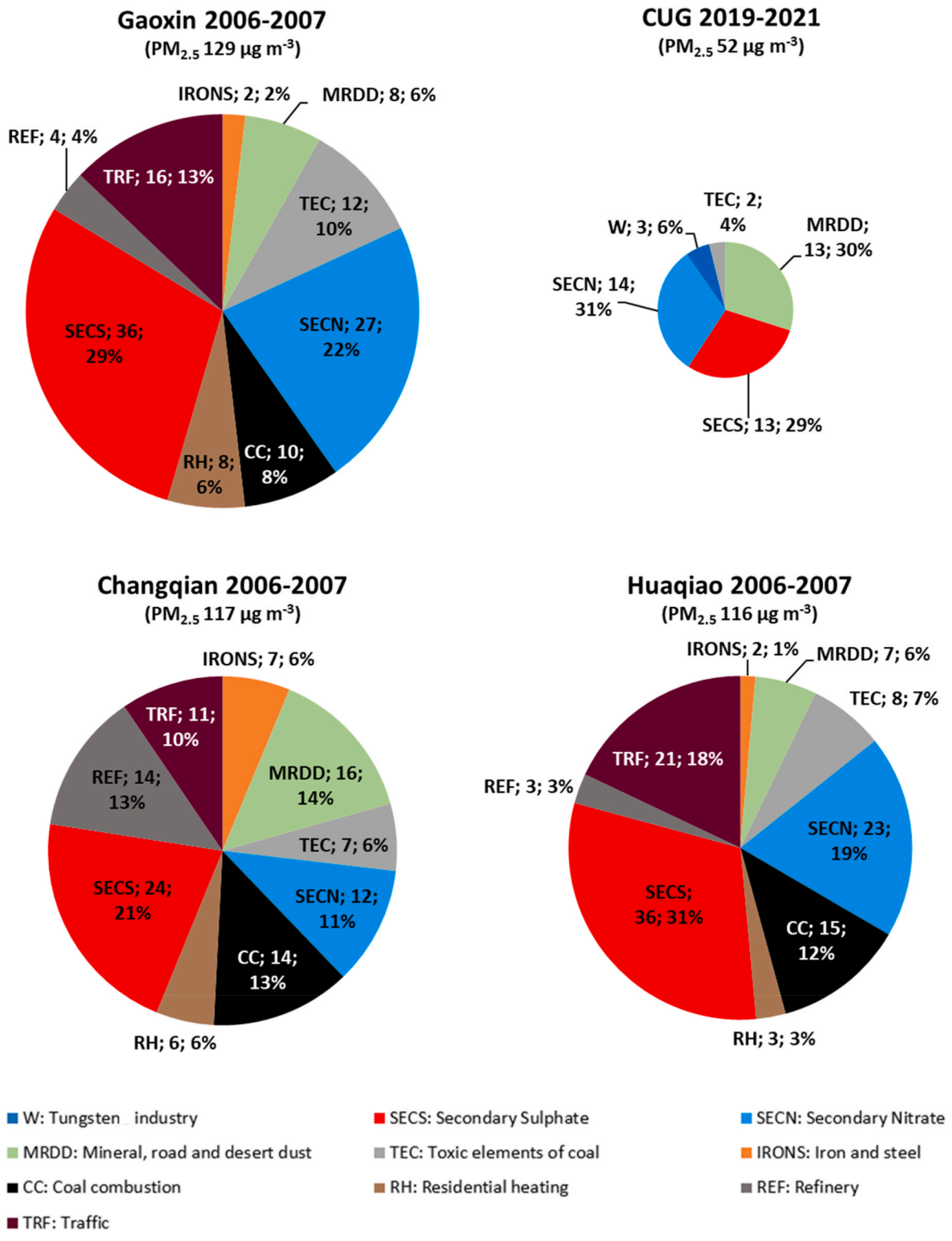

Fig. 7. Mean contributions of the nine main sources identified to the gravimetric $PM_{2.5}$ concentrations determined in 2006–2007 at all three sites (Gaoxin, Changqian and Huaqiao) and the five main sources identified in the CUG site during the 2019–2021 period, scaled by the $PM_{2.5}$ concentrations. Also shown are the $PM_{2.5}$ average concentrations and percentages for each factor and sampling site.

concentrations by 83% and 10 µg m^{-3} from the FP to the SP due to policies implemented to reduce emissions from metallurgy in Wuhan. This source contributes 4% to the $PM_{2.5}$, thus, is a minor source.

4.5.6. Traffic

This profile is identified in the FP PMF analysis, thus, is the first non-common profile. It stands for traffic (TRF) and is characterised by a composition dominated by OC (33%), SO_4^{2-} (15%), NH_4^+ (3%) and EC (2%). This factor highly contributes to the explained variation of OC, Cu and Pb (32%), followed by Sb, Cd and Zn (28%) and EC (16%). In this case, the OC/EC ratio is 13.4. This source is attributed to road traffic due to the high contributions to OC and EC from exhaust emissions, as well

as some metals from non-exhaust vehicle emissions (Amato et al., 2016). In the DISP results, the main tracers show small intervals, while SO_4^{2-}, NH_4^+, Fe, Ca, Cl^-, Mg and Pb show high DISP intervals, where they can achieve much higher concentrations. Traffic contributions are observed at all sites, although this factor has higher peaks in Huaqiao, the urban site located in the city centre and it can also be influenced by anticyclonic conditions (Ding et al., 2013). This source contributed 13% (16 μg m^{-3}) and 10–18% (11–21 μg m^{-3}) in the FP for Gaoxin, Changqian and Huaqiao, respectively.

4.5.7. Coal combustion

This is a FP-factor, the coal combustion (CC) and is characterised by a composition with high concentrations of OC (16%), Cl^- (7%), NH_4^+ (6%), and NO_3^- (5%). This factor highly contributes to the explained variation of Cl^- (65%) and, to a lesser extent, EC (21%), P (14%), OC, Cu, Na and Sb (12%). In the DISP results, main tracers show very small DISP intervals, while Al, Fe, K and SO_4^{2-} show high DISP intervals, where they could be constrained to low values without significantly affecting the fit. We attribute this source to CC, traced by Cl^- and several metals associated with it. Chloride is also likely present due to the formation of ammonium chloride in regions where high-Cl coal is burned (Li et al., 2019b). The modes of Cl occurrence in coal are varied. In fact, organic-associated Cl seems to predominate in coal. In addition, the Cl content decreases due to the decreasing sorption capacity of the highly carbonised coal organic matter (Yudovich and Ketris, 2006). This source contributed 8% (10 μg m^{-3}) and 13–12% (14–15 μg m^{-3}) in the FP for Gaoxin, Changqian and Huaqiao, respectively.

4.5.8. Residential heating

The residential heating (RH) FP-factor is characterised by a factor profile with high species concentrations of SO_4^{2-} (27%), K (14%), NO_3^- (12), OC (11%), and to a lesser extent, EC (3%). This factor contributes to the explained variation of Rb and Cs (37%), K (29%), Pb and Tl (18–21%), among others, being the source with the third-highest explained SO_4^{2-} variation. The OC/EC concentration ratio reached 3.5, which points to coal combustion emissions (Xu et al., 2015). The presence of Rb and K points to biomass burning, burning of certain metals and combustion of other materials. The nature of this source depends strongly on the nature of the fuel (Hopke et al., 2020; Zheng et al., 2018). Thus, coal combustion tracers such as SO_4^{2-}, OC, EC and Zn (Song et al., 2008) are considered in addition to waste combustion tracers (OC, EC, K, Pb, Sn) (Kumar et al., 2015). That is why we identified this source as RH, which includes biomass and waste burning. According to the DISP results, the main tracers show very small error intervals, indicating the high robustness of this factor. However, NO_3^-, Ca and Cl^- show higher variability but do not affect the stability of this factor. This factor contributes to the FP and does not show any seasonal pattern except for the higher peaks in winter months due to poor dispersion conditions. In fact, the average source contribution during the FP was 6% (8 μg m^{-3}) at Gaoxin, 6% (6 μg m^{-3}) at Changqian and 3% (3 μg m^{-3}) at Huaqiao. It is not identified as main source contributing to the $PM_{2.5}$ composition in the SP CUG site when natural gas consumption increased, even though de-centralised coal stoves and biomass stoves were still widely used by single-family homes for winter space heating in rural areas (Su et al., 2018).

4.5.9. Refinery

The factor is also a non-common profile. Namely, refinery (REF), is characterised by a profile with concentration contributions from SO_4^{2-} (5%), Al (4%), Fe (3%), OC and EC (3%), and it contributes highly to the explained variations of La (55%), Ce and V (50%), Gd (47%), Sr (36%), Se and Ti (35%), Ba (30%), Co and Al (29%), followed by Fe and Tl (17%). This pattern is clearly also a metalliferous stack emission profile, in which some of the tracers are released into the atmosphere during the refining of crude oil and processing of its downstream products in the petrochemical complex (Riccardi et al., 2008; Sánchez de la Campa et al., 2011). The Ce/La ratio is lower (1.7) than the one from MRDD (2.7), which is likely due to the contribution of La from catalytic cracking (Du and Turner, 2015). The uncertainty generated by the amount of rotational space results in a very minor rise in Q, showing small DISP intervals for the main tracers and larger intervals for NO_3^-, indicating that it could have been constrained to the base run profile with a very small change in Q. There is also variability for SO_4^{2-}, OC, NH_4^+, Ca and K; however, the factor stability is not affected. Source contributions do not show a clear seasonal pattern and are characterised by random concentration peaks. The highest contributions are at the industrial site of Changqian in the FP due to the presence of a refinery (Lv, 2008; Querol et al., 2006). This source contributed 4% (4 μg m^{-3}), 13 (14 μg m^{-3}) and 3% (3 μg m^{-3}) in the FP for Gaoxin, Changqian and Huaqiao, respectively.

4.5.10. Iron and steel

The FP-factor named iron and steel (IRONS) is characterised by high contributions of SO_4^{2-} (43%), Fe (14%) and NH_4^+ (13%. This highly contributed to the explained variation of Fe (39%), Cr (32%) and Mn (29%), followed by Se and Sr (18–23%), as well as Mg, Cu, Zn and Co (13–17%), which are considered tracers of industrial activities involving the treatment and manufacturing of steel (Querol et al., 2006). The DISP results once again show quite a robust profile with small error intervals for the main tracers. Additionally, the base run concentrations of OC, K and NO_3^- correspond to the minimum of the DISP interval. Also, SO_4^{2-}, NH_4^+, Cl^-, EC and Al show higher variabilities but did not affect the stability of this factor. This iron smelting contribution mostly impacts the industrial site of Changqian in the FP, without any trend or seasonality. This source contributed 2% (2 μg m^{-3}) at Gaoxin, 6% (7 μg m^{-3}) at Changqian and 1% (2 μg m^{-3}) at Huaqiao in the FP.

According to these results, when comparing the FP and the SP, Gaoxin and CUG sites, drastic changes can be observed in the $PM_{2.5}$ composition. The decreases of SECN, SECS and TEC (48–83% of the absolute concentrations) are attributable to policy actions implemented in the region. However, the contribution of MRDD increased by 62.5% and only 5 μg m^{-3}, likely due to the very high level of demolition/construction activities.

In relative proportions, TEC (−83%), SECS (−64%) and SECN (−48%) reduced their contributions to $PM_{2.5}$ between 2006 and 2021 whilst MRDD increased (+62.5%). The relative contributions of TRF, CC, RH, REF and IRONS where no more identified as major sources in the 2019–2020 PMF analysis. Thus, the relative contributions of nitrate-, traffic-, energy production- and industry-related $PM_{2.5}$ were markedly reduced.

5. Conclusions

This study is one of very few from China comparing experimental $PM_{2.5}$ speciation and source apportionment data from two decades ago with the current one. In this case, we performed this comparison in Wuhan (a megacity located in central China).

Air quality in this megacity has improved considerably over the last 15 years. In this study, air quality monitoring data and $PM_{2.5}$ speciation datasets obtained during the 2006–2007 and 2019–2021 periods were employed to evaluate the major causes (decreased source contributions) that accounted for the marked decreases in $PM_{2.5}$ and to describe major targets (dominant source contributions) to continue abating PM pollution.

Average SO_2 concentrations decreased by 88% from the first to the SP, mostly due to measures and reduction in CC. However, NO_2 concentrations were only reduced by 25%, with the success of pollution abatement measures likely being affected by the increased number of vehicles. $PM_{2.5}$ concentrations decreased by 65%, with PM components being affected differently. Thus, CC-related elements, such as Pb, Ni, Ga, Rb, As, Tl, Se, Sn, Bi, K and Zn, decreased concentrations by 76–90%, while OC, SO_4^{2-}, NH_4^+, EC and Cl^- decreased concentrations by 48–71%,

and Al, Ca, Cu, Fe and Co, as well as NO_3^-, reduced concentrations by 22–54 and 22%, respectively. The secondary inorganic aerosol (SIA) was composed of 73% $(NH_4)_2SO_4$ in 2006, while NH_4NO_3 prevailed in 2021 with 52%.

Currently, the major source contributions to $PM_{2.5}$ in Wuhan's urban background in 2019–2020 were SECN (31%), MRDD (30%), SECS (29%), W (6%) and TEC (4%).

The results indicate a drastic abatement of PM pollution in Wuhan, as well as a change of sources to focus on the continued abatement of $PM_{2.5}$ concentrations. Based on the current $PM_{2.5}$ composition, the secondary inorganic aerosols (SO_4^{2-}, NO_3^- and NH_4^+) are the major components, followed by organic matter. All together accounting for at least 65% of $PM_{2.5}$. On the other side, the results of the source apportionment show that regional secondary $PM_{2.5}$ (secondary sulphate, nitrate, ammonium and secondary organic aerosols) are the major source contributors, with 60% of $PM_{2.5}$, followed by mineral matter sources (30%) from construction, demolition, road dust and desert dust. These results suggest that efforts should be done in reducing more the emissions of inorganic and organic precursors of secondary PM (SO_2, NOx, NH_3 and VOCs) to efficiently abate $PM_{2.5}$ in Wuhan, but also abatement of fugitive dust emissions should receive a major focus for policy measures.

In future research, organic molecular markers will be used to complete and improve the existing $PM_{2.5}$ source apportionment analysis.

Author statement

Anna Canals-Angerri: Conceptualization, Software, Formal analysis, Investigation, Resources, Writing – original draft, Writing – review & editing, Visualization. Wei wei Lv: Conceptualization, Resources. Xinguo Zhuang: Writing – review & editing. Yunfei Shangguan: Resources, Writing – review & editing. Yanxin Wang: Writing – review & editing. Shaofei Kong: Resources, Writing – review & editing. Philip K. Hopke: Software, Formal analysis, Validation, Writing – review & editing. Fulvio Amato: Writing – review & editing. Andres Alastuey: Funding acquisition, Writing – review & editing. Barend Leendert van Drooge: Writing – review & editing. Xavier Querol: Conceptualization, Methodology, Writing – original draft, Supervision, Project administration, Funding acquisition.

Declaration of competing interest

The authors declare that they have no known competing financial interests or personal relationships that could have appeared to influence the work reported in this paper.

Data availability

Data will be made available on request.

Acknowledgements

This research was supported by the National Nature Science Foundation of China (Nos. 41972179, 41972180); the European Union's Horizon 2020 research and innovation program under grant agreement 101036245 (RI-URBANS); and the Generalitat de Catalunya (AGAUR 2021 SGR 00447). The authors would like to express our gratitude to the NOAA Air Resources Laboratory (ARL) for the provision of the HYSPLIT transport and dispersion model.

Appendix A. Supplementary data

Supplementary data to this article can be found online at https://doi.org/10.1016/j.envpol.2023.122803.

References

Amato, F., Alastuey, A., Karanasiou, A., Lucarelli, F., Nava, S., Calzolai, G., Severi, M., Becagli, S., Gianelle, V.L., Colombi, C., Alves, C., Custódio, D., Nunes, T., Cerqueira, M., Pio, C., Eleftheriadis, K., Diapouli, E., Reche, C., Minguillón, M.C., Manousakas, M.I., Maggos, T., Vratolis, S., Harrison, R.M., Querol, X., 2016. AIRUSE-LIFE+: a harmonized PM speciation and source apportionment in five southern European cities. Atmos. Chem. Phys. 16, 3289–3309. https://doi.org/10.5194/acp-16-3289-2016.

Amato, F., Pandolfi, M., Escrig, A., Querol, X., Alastuey, A., Pey, J., Perez, N., Hopke, P. K., 2009. Quantifying road dust resuspension in urban environment by Multilinear Engine: a comparison with PMF2. Atmos. Environ. 43, 2770–2780. https://doi.org/10.1016/j.atmosenv.2009.02.039.

Arruti, A., Fernández-Olmo, I., Irabien, A., 2011. Impact of the global economic crisis on metal levels in particulate matter (PM) at an urban area in the Cantabria Region (Northern Spain). Environ. Pollut. 159, 1129–1135. https://doi.org/10.1016/j.envpol.2011.02.008.

Birch, M.E., Cary, R.A., 1996. Elemental carbon-based method for monitoring occupational exposures to particulate diesel exhaust. Aerosol Sci. Technol. 25, 221–241. https://doi.org/10.1080/02786829608965393.

Brewer, J.P., Shirrow, G., 1975. In: Riley (Ed.), Chemical Oceanography. Academic Press, New York. https://doi.org/10.1016/S0422-9894(08)70141-7.

Cavalli, F., Viana, M., Yttri, K.E., Genberg, J., Putaud, J.-P., 2010. Toward a standardised thermal-optical protocol for measuring atmospheric organic and elemental carbon: the EUSAAr protocol. Atmos. Meas. Tech. 3, 79–89. https://doi.org/10.1080/00223348708572555.

Cheng, H., Gong, W., Wang, Z., Zhang, F., Wang, X., Lv, X., Liu, J., Fu, X., Zhang, G., 2014. Ionic composition of submicron particles (PM1.0) during the long-lasting haze period in January 2013 in Wuhan, central China. J. Environ. Sci. (China) 26, 810–817. https://doi.org/10.1016/S1001-0742(13)60503-3.

Chinese Meteorological Industry standard QX/T479, 2019. $PM_{2.5}$ meteorological condition assessment index (EMI). In: People's Republic of China Meteorological Industry Standard. Meteorological Publishing House., Beijing.

Dai, Q., Bi, X., Song, W., Li, T., Liu, B., Ding, J., Xu, J., Song, C., Yang, N., Schulze, B.C., Zhang, Y., Feng, Y., Hopke, P.K., 2019. Residential coal combustion as a source of primary sulfate in Xi'an, China. Atmos. Environ. 196, 66–76. https://doi.org/10.1016/j.atmosenv.2018.10.002.

Ding, A.J., Fu, C.B., Yang, X.Q., Sun, J.N., Zheng, L.F., Xie, Y.N., Herrmann, E., Nie, W., Petäjä, T., Kerminen, V.M., Kulmala, M., 2013. Ozone and fine particle in the western Yangtze River Delta: an overview of 1 yr data at the SORPES station. Atmos. Chem. Phys. 13, 5813–5830. https://doi.org/10.5194/acp-13-5813-2013.

Du, L., Turner, J., 2015. Using $PM_{2.5}$ lanthanoid elements and nonparametric wind regression to track petroleum refinery FCC emissions. Sci. Total Environ. 529, 65–71. https://doi.org/10.1016/j.scitotenv.2015.05.034.

GBD, 2020. Global burden of 87 risk factors in 204 countries and territories, 1990–2019: a systematic analysis for the Global Burden of Disease Study 2019. Lancet 396, 1223–1249. https://doi.org/10.1016/S0140-6736(20)30752-2.

Ge, J.M., Huang, J.P., Xu, C.P., Qi, Y.L., Liu, H.Y., 2014. Characteristics of Taklimakan dust emission and distribution: a satellite and reanalysis field perspective. J. Geophys. Res. Atmos. 119, 11772–11783. https://doi.org/10.1002/2013JD021040.Received.

Geng, G., Xiao, Q., Liu, S., Liu, X., Cheng, J., Zheng, Y., Xue, T., Tong, D., Zheng, B., Peng, Y., Huang, X., He, K., Zhang, Q., 2021. Tracking air pollution in China: near real-time $PM_{2.5}$ retrievals from multisource data fusion. Environ. Sci. Technol. 55, 12106–12115. https://doi.org/10.1021/acs.est.1c01863.

Harrison, R.M., Pio, C.A., 1983. Size-differentiated composition of inorganic atmospheric aerosols of both marine and polluted continental origin. Atmos. Environ. 17, 1733–1738. https://doi.org/10.1016/0004-6981(83)90180-4.

Haynes, W.M., Lide, D.R., B.T, J., 2017. In: Haynes, W.M., Lide, D.R., B.T, J. (Eds.), CRC Handbook of Chemistry and Physics, 97th Edition, p. 488. https://doi.org/10.1201/9781315380476.

Hopke, P.K., Dai, Q., Li, L., Feng, Y., 2020. Global review of recent source apportionments for airborne particulate matter. Sci. Total Environ. 740, 140091 https://doi.org/10.1016/j.scitotenv.2020.140091.

Kim, E., Hopke, P.K., 2008. Source characterization of ambient fine particles at multiple sites in the Seattle area. Atmos. Environ. 42, 6047–6056. https://doi.org/10.1016/j.atmosenv.2008.03.032.

Köppen, W., Geiger, R., 1936. Handbook of Climatology: Das geographische System der Klimate. Borntraeger Science Publishers, Berlin. https://doi.org/10.2307/200498.

Kumar, S., Aggarwal, S.G., Gupta, P.K., Kawamura, K., 2015. Investigation of the tracers for plastic-enriched waste burning aerosols. Atmos. Environ. 108, 49–58. https://doi.org/10.1016/j.atmosenv.2015.02.066.

Li, T., Li, J., Jiang, H., Chen, D., Zong, Z., Tian, C., Zhang, G., 2020. Source apportionment of $PM_{2.5}$ in guangzhou based on an approach of combining positive matrix factorization with the bayesian mixing model and radiocarbon. Atmosphere 11, 1–9. https://doi.org/10.3390/atmos11050512.

Li, X., Han, J., Hopke, P.K., Hu, J., Shu, Q., Chang, Q., Ying, Q., 2019a. Quantifying primary and secondary humic-like substances in urban aerosol based on emission source characterization and a source-oriented air quality model. Atmos. Chem. Phys. 19, 2327–2341. https://doi.org/10.5194/acp-19-2327-2019.

Li, X., Yang, K., Han, J., Ying, Q., Hopke, P.K., 2019b. Sources of humic-like substances (HULIS) in $PM_{2.5}$ in Beijing: receptor modeling. Tjyybjb.Ac.Cn 27, 58–66.

Liu, Y., Li, X., Wang, W., Yin, B., Gao, Y., Yang, X., 2020. Chemical characteristics of atmospheric PM_{10} and $PM_{2.5}$ at a rural site of Lijiang city, China. Int. J. Environ. Res. Publ. Health 17, 1–16. https://doi.org/10.3390/ijerph17249553.

Lv, W., 2008. Environmental Geochemistry and Source Apportionment of $PM_{2.5}$ in Wuhan City, Central China [Unpublished Doctoral Dissertation]. China University of Geosciencies - Wuhan (available under request).
Meng, Z., Lin, W., Zhang, R., Han, Z., Jia, X., 2017. Summertime ambient ammonia and its effects on ammonium aerosol in urban Beijing, China. Sci. Total Environ. 579, 1521–1530. https://doi.org/10.1016/j.scitotenv.2016.11.159.
MEP, 2012. GB 3095-2012: Ambient Air Quality Standards. Ministry of Environmental Protection of the People's Republic of China.
NMIC, 2022. Map of China's Surface Climate (1981-2010). National Meteorological Information Center.
Paatero, P., 1997. Least squares formulation of robust non-negative factor analysis. Chemometr. Intell. Lab. Syst. 37, 23–35.
Paatero, P., Eberly, S., Brown, S.G., Norris, G.A., 2014. Methods for estimating uncertainty in factor analytic solutions. Atmos. Meas. Tech. 7, 781–797. https://doi.org/10.5194/amt-7-781-2014.
Paatero, P., Hopke, P.K., 2003. Discarding or downweighting high-noise variables in factor analytic models. Anal. Chim. Acta 490, 277–289. https://doi.org/10.1016/S0003-2670(02)01643-4.
Paatero, P., Tapper, U., 1994. Positive matrix factorization: a non-negative wiht optimal utilization of error estimates of data values. Environmetrics 5, 111–126.
Pacyna, J.M., Ottar, B., Tomza, U., Maenhaut, W., 1985. Long-range transport of trace elements to Ny Ålesund. Spitsbergen. Atmos. Environ. 19, 857–865. https://doi.org/10.1016/0004-6981(85)90231-8.
Qian, W., Tang, X., Quan, L., 2004. Regional characteristics of dust storms in China. Atmos. Environ. 38, 4895–4907. https://doi.org/10.1016/j.atmosenv.2004.05.038.
Qin, D.H., 1995. A Study of Present Climatic and Environmental Record in the Surface Snow of the Antarctic Ice Sheet. Sci. Press.
Qin, S., Kong, S., Wu, J., Liu, X., Cheng, Y., Wu, F., Niu, Z., Liu, J., Feng, Y., Yan, Y., Qi, S., 2020. Spatial-temporal diversities of ammonia emissions and impacting factors in Hubei Province from 1996 to 2016. China Environ. Sci. 4, 1403–1413. https://doi.org/10.19674/j.cnki.issn1000-6923.2020.0155.
Querol, X., Alastuey, A., Rodriguez, S., Plana, F., Ruiz, C.R., Cots, N., Massagué, G., Puig, O., 2001. PM_{10} and $PM_{2.5}$ source apportionment in the Barcelona Metropolitan area, Catalonia, Spain. Atmos. Environ. 35, 6407–6419. https://doi.org/10.1016/S1352-2310(01)00361-2.
Querol, X., Zhuang, X., Alastuey, A., Viana, M., Lv, W., Wang, Y., López, A., Zhu, Z., Wei, H., Xu, S., 2006. Speciation and sources of atmospheric aerosols in a highly industrialised emerging mega-city in Central China. J. Environ. Monit. 8, 1049–1059. https://doi.org/10.1039/b608768j.
Ren, Z., Liu, X., Liu, T., Chen, D., Jiao, K., Wang, X., Suo, J., Yang, H., Liao, J., Ma, L., 2021. Effect of ambient fine particulates ($PM_{2.5}$) on hospital admissions for respiratory and cardiovascular diseases in Wuhan, China. Respir. Res. 22, 1–11. https://doi.org/10.1186/s12931-021-01731-x.
Riccardi, C., Di Filippo, P., Pomata, D., Incoronato, F., Di Basilio, M., Papini, M.P., Spicaglia, S., 2008. Characterization and distribution of petroleum hydrocarbons and heavy metals in groundwater from three Italian tank farms. Sci. Total Environ. 393, 50–63. https://doi.org/10.1016/j.scitotenv.2007.12.010.
Rothenberg, S.E., Windham-Myers, L., Creswell, J.E., 2014. Rice methylmercury exposure and mitigation: a comprehensive review. Environ. Res. 133, 407–423. https://doi.org/10.1016/j.envres.2014.03.001.
Sánchez de la Campa, A.M., Moreno, T., de la Rosa, J., Alastuey, A., Querol, X., 2011. Size distribution and chemical composition of metalliferous stack emissions in the San Roque petroleum refinery complex, southern Spain. J. Hazard Mater. 190, 713–722. https://doi.org/10.1016/j.jhazmat.2011.03.104.
Senior, C., Granite, E., Linak, W., Seames, W., 2020. Chemistry of trace inorganic elements in coal combustion systems: a century of discovery. Energy Fuel. 34, 15141–15168. https://doi.org/10.1021/acs.energyfuels.0c02375.
Silver, B., He, X., Arnold, S.R., Spracklen, D.V., 2020. The impact of COVID-19 control measures on air quality in China. Environ. Res. Lett. 15 https://doi.org/10.3390/su14137853.
Soba, D., Gámez, A.L., Becerril, J.M., Esteban, R., Aranjuelo, I., 2022. Traffic restrictions during COVID-19 lockdown improve air quality and reduce metal biodeposition in tree leaves. Urban For. Urban Green. 70 https://doi.org/10.1016/j.ufug.2022.127542.
Song, Y., Dai, W., Wang, X., Cui, M., Su, H., Xie, S., Zhang, Y., 2008. Identifying dominant sources of respirable suspended particulates in Guangzhou, China. Environ. Eng. Sci. 25, 959–968. https://doi.org/10.1089/ees.2007.0146.
Stein, A.F., Draxler, R.R., Rolph, G.D., Stunder, B.J.B., Cohen, M.D., Ngan, F., 2015. Noaa's hysplit atmospheric transport and dispersion modeling system. Bull. Am. Meteorol. Soc. 96, 2059–2077. https://doi.org/10.1175/BAMS-D-14-00110.1.
Su, C., Madani, H., Palm, B., 2018. Heating solutions for residential buildings in China: current status and future outlook. Energy Convers. Manag. 177, 493–510. https://doi.org/10.1016/j.enconman.2018.10.005.
WEEB, 2021. Bulletin of the Second National Survey of Pollution Sources in Wuhan in 2017 [WWW Document]. URL. http://hbj.wuhan.gov.cn/hjsj/ztzl/decwrypc/index.shtml#book7/page1.
WHO, 2022. WHO's Global Health Observatory. 2010-2016 Dataset on $PM_{2.5}$ Concentrations by Country [WWW Document]. URL. https://www.who.int/data/gho/data/indicators/indicator-details/GHO/concentrations-of-fine-particulate-matter-(pm2-5.
WHO, 2021. WHO Global Air Quality Guidelines: Particulate Matter ($PM_{2.5}$ and PM_{10}); Ozone; Nitrogen Dioxide; Sulphur Dioxide and Carbon Monoxide. Coastal And Estuarine Processes.
WHO, 2013. Review of Evidence on Health Aspects of Air Pollution - REVIHAAP Project. World Health Organization Regional Office for Europe 2013. Technical Report.
World Bank, 2016a. The GDP World Bank Annual Report 2016. Washington, DC.
World Bank, 2016b. The Cost of Air Pollution, the Cost of Air Pollution. World Bank, Washington, DC. https://doi.org/10.1596/25013.
Wuhan Council, 2021. Communiqué of the Seventh National Population Census of Wuhan City. No. 6).
Xu, H., Guinot, B., Shen, Z., Ho, K.F., Niu, X., Xiao, S., Huang, R.J., Cao, J., 2015. Characteristics of organic and elemental carbon in $PM_{2.5}$ and PM0.25 in indoor and outdoor environments of a middle school: secondary formation of organic carbon and sources identification. Atmosphere 6, 361–379. https://doi.org/10.3390/atmos6030361.
Yin, Z., Huang, X., He, L., Cao, S., Zhang, J.J., 2020. Trends in ambient air pollution levels and $PM_{2.5}$ chemical compositions in four Chinese cities from 1995 to 2017. J. Thorac. Dis. 12, 6396–6410. https://doi.org/10.21037/jtd-19-crh-aq-004.
Yu, L., Wang, G., Zhang, R., Zhang, L., Song, Y., Wu, B., Li, X., An, K., Chu, J., 2013. Characterization and source apportionment of $PM_{2.5}$ in an urban environment in Beijing. Aerosol Air Qual. Res. 13, 574–583. https://doi.org/10.4209/aaqr.2012.07.0192.
Yudovich, Y.E., Ketris, M.P., 2006. Chlorine in coal: a review. Int. J. Coal Geol. 67, 127–144. https://doi.org/10.1016/j.coal.2005.09.004.
Zhai, S., Jacob, D.J., Wang, X., Shen, L., Li, K., Zhang, Y., Gui, K., Zhao, T., Liao, H., 2019. Fine particulate matter ($PM_{2.5}$) trends in China, 2013-2018. separating contributions from anthropogenic emissions and meteorology. Atmos. Chem. Phys. 19, 11031–11041. https://doi.org/10.5194/acp-19-11031-2019.
Zhang, Z., Yan, Y., Kong, S., Deng, Q., Qin, S., Yao, L., Zhao, T., Qi, S., 2022. Benefits of refined NH3 emission controls on $PM_{2.5}$ mitigation in Central China. Sci. Total Environ. 814 https://doi.org/10.1016/j.scitotenv.2021.151957.
Zheng, B., Tong, D., Li, M., Liu, F., Hong, C., Geng, G., Li, H., Li, X., Peng, L., Qi, J., Yan, L., Zhang, Y., Zhao, H., Zheng, Y., He, K., Zhang, Q., 2018. Trends in China's anthropogenic emissions since 2010 as the consequence of clean air actions. Atmos. Chem. Phys. 18, 14095–14111. https://doi.org/10.5194/acp-18-14095-2018.
Zhou, C.-H., Gong, S., Zhang, X.-Y., Liu, H.-L., Xue, M., Cao, G.-L., An, X.-Q., Che, H.-Z., Zhang, Y.-M., Niu, T., 2012. Towards the improvements of simulating the chemical and optical properties of Chinese aerosols using an online coupled model – CUACE/Aero. Tellus B 64, 18965. https://doi.org/10.3402/tellusb.v64i0.18965.
Zhou, J., Huang, Y., Qiu, P., Liu, H., Xiao, K., 2018. Study on emission inventory and distribution characteristics of air pollution sources in wuhan 2014. J. Nanjing Univ. Inf. Technol. (Natural Sci. Ed. 599–605. https://doi.org/10.13878/j.cnki.jnuist.2018.05.010.
Zíková, N., Wang, Y., Yang, F., Li, X., Tian, M., Hopke, P.K., 2016. On the source contribution to Beijing $PM_{2.5}$ concentrations. Atmos. Environ. 134, 84–95. https://doi.org/10.1016/j.atmosenv.2016.03.047.